Molecular Crystals and Liquid Crystals

ISSN: 1542-1406 (Print) 1563-5287 (Online) Journal homepage: http://www.tandfonline.com/loi/gmcl20

Reversible Photo Actuated Bulk Nanocomposite with Nematic Liquid Crystalline Elastomer Matrix

Chensha Li, Xuezhen Huang, Chenhui Li & Hongrui Jiang

To cite this article: Chensha Li, Xuezhen Huang, Chenhui Li & Hongrui Jiang (2015) Reversible Photo Actuated Bulk Nanocomposite with Nematic Liquid Crystalline Elastomer Matrix, Molecular Crystals and Liquid Crystals, 608:1, 146-156, DOI: 10.1080/15421406.2014.953748

To link to this article: http://dx.doi.org/10.1080/15421406.2014.953748

Mol. Cryst. Liq. Cryst., Vol. 608: pp. 146–156, 2015

ISSN: 1542-1406 print/1563-5287 online
DOI: 10.1080/15421406.2014.953748

Reversible Photo Actuated Bulk Nanocomposite with Nematic Liquid Crystalline Elastomer Matrix

CHENSHA LI,[1,2,*] XUEZHEN HUANG,[1] CHENHUI LI,[1] AND HONGRUI JIANG[1,3,*]

[1]Department of Electrical and Computer Engineering, University of Wisconsin-Madison, Madison, WI, USA
[2]Department of Materials Science, Harbin Engineering University, Harbin, China
[3]Materials Science Program, University of Wisconsin-Madison, Madison, WI, USA

Liquid crystal elastomers (LCEs) are excellent actuator materials. However, current LCE materials are generally made in the forms with thin thickness, such as films or fibers, which have limitations in forming actuators. We have developed a bulk LCE material with the three-dimensional elastic skeleton network of polyurethane and the matrix of nematic LCE incorporating single-wall carbon nanotubes (SWCNTs). This LCE nanocomposite bulk (LCENB) exhibited sensitive and reversible photo actuation. It could evenly contract by up to 25% of the initial height under a uniform irradiation, or bend towards the incident light by up to 40° under an asymmetrical irradiation. A photo-driven scanning mirror with superior scanning angle, implementing this LCENB as the actuator, was also demonstrated.

Keywords Carbon nanotubes; liquid crystal elastomers; nanocomposites; deformation; photo actuation

1. Introduction

Actuator materials with the capability of change in shape and dimensions upon a given stimulus, such as the electric field, temperature or light, attract great attention recently owing to their novel and wide-range applications in manufacturing, consumer products, and health care [1–4]. To achieve actuators as elegant as human muscles, soft polymer actuator materials are especially promising due to their high mechanical flexibility, light weight, low costs, and low-noise operation [5]. Among these soft polymer actuator materials, liquid crystal elastomers (LCEs) are excellent candidates because they possess properties of both liquid crystals and elastomers, owing to the self-assembly of mesogenic groups and weak density of polymeric chain reticulation that leads to rubber elasticity [6]. Both of these attributes are critical for the fabrication of reversible actuators with large dimensional

Chensha Li and Xuezhen Huang contributed equally to this work.

*Address correspondence to Hongrui Jiang and Chensha Li, Department of Electrical and Computer Engineering, University of Wisconsin-Madison, 1415 Engineering Drive, Madison, WI 53706, USA; E-mail: hongrui@engr.wisc.edu; lichnsa@mail.tsinghua.edu.cn

Color versions of one or more of the figures in the article can be found online at www.tandfonline.com/gmcl.

changes [4–8]. Owing to their characteristics as soft materials, currently, LCE materials have always been made in the forms with thin thickness, such as films [9–24], fibers [25–28] or applied as surface coating [29]. However, materials with thin thickness have limitations in forming mechanical actuators, and many actuation functions need to be realized using thick materials, such as bulk materials. Therefore, it is highly desirable to develop bulk LCE materials that can function as actuators.

In previously reported LCE composite films, hetero polymer networks were utilized as the frame to form the alignment of liquid crystalline units, or as reinforcement phase to accomplish good mechanical properties [21, 22]. Leveraging this approach, incorporating hetero skeleton structures can be an effective way of developing bulk LCE materials. In this work, we developed an LCE material with a bulk structure, with a three-dimensional (3D) elastic skeleton network of polyurethane and a nematic LCE filled with single-wall carbon nanotubes (SWCNTs) as the matrix. The resultant LCE nanocomposite bulk (LCENB) could be reversibly actuated by light with high sensitivity. We chose light as the stimulus for the activation of the LCENB since light is a clean energy source and can be controlled rapidly and remotely, and light-driven actuators have shown many promising applications [10, 17]. Incorporating nanophase materials with the function of photo-thermal conversion into LCE matrices is a widely adopted method for photo actuated LCE materials [30], LCE materials actuated in such a way are called photo-thermo-mechanically actuated LCE materials [31]. Compared with those LCE materials whose actuations are induced by the photoresponse of the photochromic groups incorporated into the LCE network and where the photo-actuation is generally generated in the surface layer of the materials, the actuation of photo-thermo-mechanically actuated LCE materials can generally occur much deeper into the materials [32]. Hence, the materials can be made into thicker forms. We have developed our LCENB based on photo-thermo-mechanically actuated LCE materials. Our LCENB could contract evenly by up to 25% of its initial height under a uniform irradiation, or bend towards the light source by up to 40° under asymmetric irradiation. We further demonstrated a photo-driven scanning mirror based on our LCENB. The scanning mirror showed superior performance with large scanning range.

2. Experimental Procedures

Materials Preparation

The pendant mesogenic group, 4-methoxyphenyl-4-(1-buteneoxy) benzoate, and di-functional crosslinking group, 1, 4 alkeneoxybenzene, were synthesized as reported in our prior work [16]. The polymer backbone was a poly-methylhydrosiloxane (PMHS) with approximately 60 Si–H units per chain, obtained from ACROS Chemicals (Geel, Belgium). The commercial platinum catalyst dichloro(1, 5-cyclooctadiene) platinum(II), was obtained from Sigma-Aldrich (St Louis, MO, USA). The catalyst solution was prepared by dissolving 0.025 g of the dichloro(1, 5-cyclooctadiene) platinum(II) in 2 mL of dichloromethane, then adding 20 mL of toluene. The polyurethane porous foam was obtained from Hengda Company (Beijing, China), the average aperture was about 0.4 mm.

The synthesis of the side-chain nematic LCE network with the polysiloxane backbone was via a sol-gel method through a two-stage crosslinking, coupled with a drawing process. The Si–H bonds in the polysiloxane backbone reacted, using the platinic acid catalyst, with the terminal vinyl groups of the mesogenic rod-like molecules and the two-functional

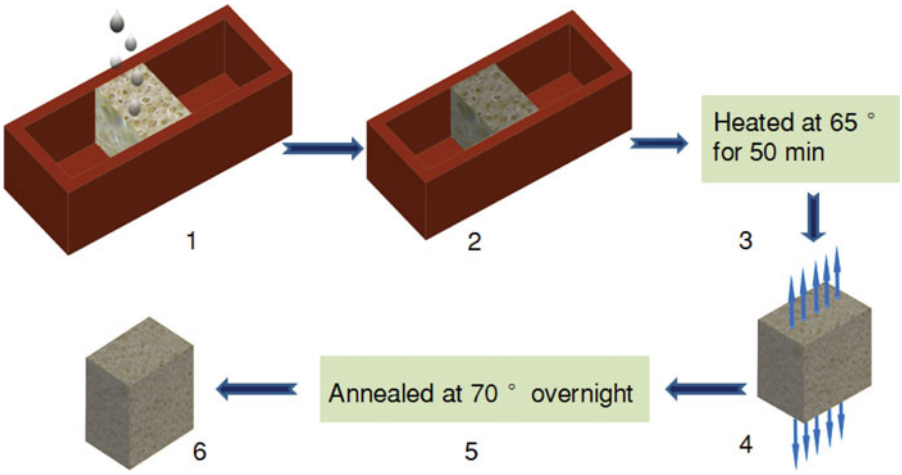

Figure 1. Schematic of the fabrication process of the LCENB with the 3D elastic skeleton network of polyurethane and the nematic LCE/SWCNT as the matrix. (1) Casting reaction solution mixture into a mold with the polyurethane porous foam inserted into it. (2) Reaction solution mixture is absorbed and held inside the polyurethane porous foam; the solution is sufficient to soak the polyurethane porous rubber without any overflow. (3) The first crosslinking. (4) The drawing process. (5) The second crosslinking. (6) The completed LCENB.

crosslinkers by hydrosilation, achieving the 10:1 ratio of substituted groups on each chain, or an effective 9% cross-linking density.

The fabrication of the LCENB, consisting of the 3D elastic skeleton network of polyurethane and the side-chain nematic LCE incorporated with SWCNTs as the matrix, was based on the above described process. The fabrication process is shown in Fig. 1. A polyurethane porous foam was cut to be a cuboid bulk with the height, width and thickness of 1.8 cm, 1.0 cm, and 0.7 cm, respectively. This cuboid bulk of polyurethane porous foam was squeezed into a polytetrafluoroethylene (PTFE) rectangular parallel-piped mold whose length, depth, and width were 6 cm, 1 cm, and 1.6 cm, respectively. The direction along the height of the polyurethane porous foam bulk was parallel to that of the width of the PTFE mold. Therefore, the top and bottom surfaces of the polyurethane porous foam were in close contact with the two sides of the mold. A 1 mg of SWCNTs were mixed into the reaction mixture solution, which was 0.06 g of PMHS, 0.25 g of 4-methoxyphenyl-4-(1-buteneoxy) benzoate (0.84 mmol), and 0.034 g of 1, 4 alkeneoxybenzene (0.083 mmol) solved in 1 mL of toluene, ultrasonicated for 2 min to ensure homogeneous dispersion. A 50 μL of catalyst solution was then added into the reaction mixture solution containing SWCNTs. Next, the solution was cast into the PTFE mold. The solution was fully absorbed into the polyurethane porous foam and was held inside it by the capillary force. This specified volume of the prepared solution could adequately soak the polyurethane porous foam without overflowing outside. The mold was subsequently covered by a cap and heated in an oven at 65°C for 50 min for partial crosslinking (first crosslinking stage). Then, the mold was cooled down to the room temperature. The polyurethane porous foam was carefully removed from the mold and placed on a glass slide. The LCE matrix was held in the inter pores of the 3D polyurethane skeleton network, which not only serves as a mechanical reinforcement matrix, but also would effectively exert its elasticity to assist

in the reversible actuation process. From the material synthesis perspective, the utilization of polyurethane skeleton network as a full 3D elastic scaffold here is a key advance compared with the polyurethane fiber-network/SWCNT/LCE composite films reported in our previous work [22]. After this first stage of crosslinking, the pores of the polyurethane porous foam were fully filled by the partially crosslinked swollen gel incorporated with SWCNTs. As the toluene contained in the gel was gradually evaporated, the gel shrank in the process and forcing the elastic polyurethane porous foam to shrink together. After 40 min of this drying process, the nanocomposite bulk contracted to a stable height of about 1.1 cm. Then, the drawing process started, in which the top edge and bottom edge of the nanocomposite bulk were each pierced with five equally spaced hooks made of copper wires. The nanocomposite bulk was hung utilizing the top five copper hooks. Five loads, each 7 g in weight, were attached to the five copper hooks at the bottom, respectively. After 12 hr of the gradual uniaxial stretch along the height by the loads, the nanocomposite bulk was extended to a stable height of 1.6 cm, which was its initial height framed by the PTFE mold, and a nematic alignment in the partially crosslinked gel matrix was obtained. Then, the nanocomposite bulk with the loads was annealed at 70°C overnight to complete the crosslinking reaction in the nematic phase (second crosslinking stage). This completed the preparation of the LCENB with 3D elastic skeleton of polyurethane and the nematic LCE incorporated with SWCNTs (with SWCNT content of 0.3 wt%) as the matrix. The LCENB had dimensions of 1.6 cm $\times$ 0.8 cm $\times$ 0.6 cm. The weight ratio of polyurethane skeleton to the LCE matrix was about 1:4.

Characterization Methods

The LCENB was studied under a polarizing optical microscope (Nikon Instruments, SMZ 1500, Melville, NY) and an X-ray diffraction spectra by a Bruker/Siemens Hi-Star 2d X-ray Diffractometer with a monochromatic CuKalpha point source (0.8 mm). A slice, 1 mm in thickness, cut from the LCENB along the plane parallel to its height and width, was used to measure the X-ray diffraction spectra. The photo-actuation measurements of the LCENB were performed utilizing either an IR source (HOT SPOT: HS 250.3, 250 Watt) or a white light source (New Port, Oriel Productline, Model 66885, Irvine, CA, USA). The temperature change of the LCENB in response to the light stimulus was tested by a multilogger thermometer (HH 506 RA, OMEGA Engineering, Stamford, CT). The detector, with the dimension of 2 mm in length and 100 μm in diameter, was placed on the sample surfaces.

3. Results and Discussions

Polysiloxane-based nematic LCEs, one of the main categories of LCE materials, are generally synthesized by the sol-gel method based on the procedure of two-stage crosslinking coupled with a drawing process that forms alignments in the LCE networks [8]. In this work, such a synthesis process was leveraged to fabricate the nematic LCENB. Depending on the capillarity, the polyurethane porous foam saturated held the reaction mixture solution inside its pore spaces, leading to the synthesis of the LCE within the 3D network of polyurethane. The obtained nematic LCENB consisted of a 3D elastic skeleton network of polyurethane and a polysiloxane-based side-chain nematic LCE incorporating SWCNTs as the matrix.

The microscopic image in Fig. 2(a) indicates that the as-prepared LCENB maintains the porous structure formed by the polyurethane porous foam (as shown in Fig. S1(a)), while the polyurethane skeleton was tightly cladded by the LCE/SWCNT matrix. The

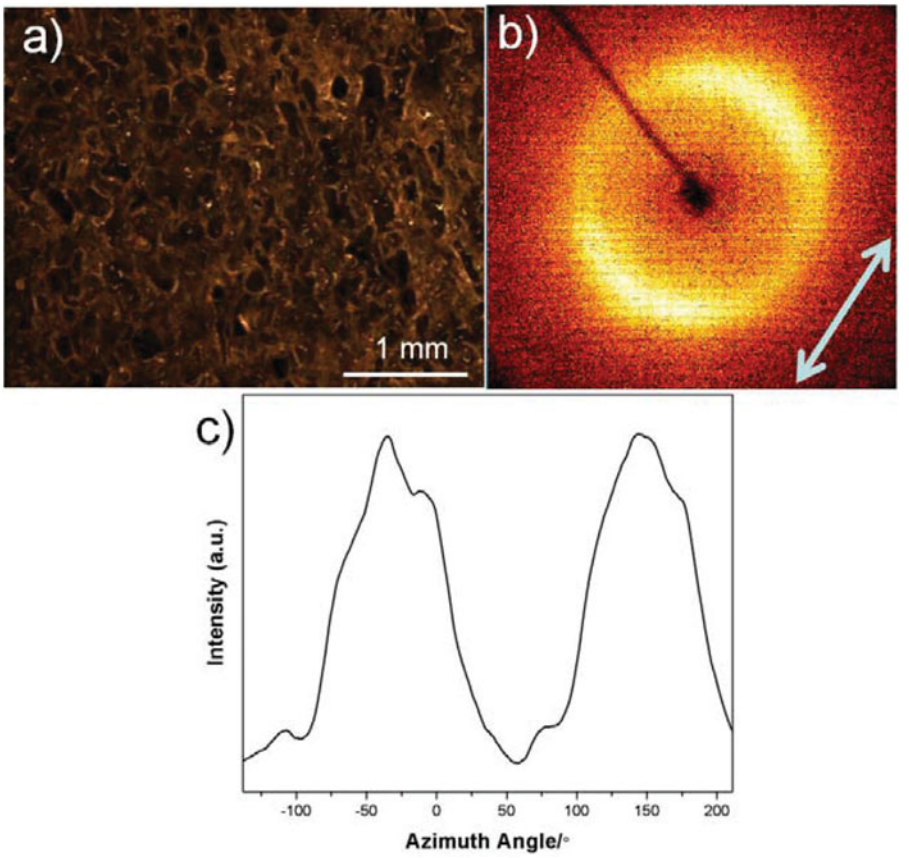

Figure 2. (a) A microscopic photograph of the prepared LCENB. (b) An X-ray diffraction pattern obtained from the LCENB. Black line indicates the 0° azimuth angle; white arrow shows the direction perpendicular to the alignment orientation of mesogens in the LCE network. (c) Azimuthal intensity distribution of the X-ray diffraction pattern.

anisotropic alignment of mesogens in the LCE matrix of the bulk was proved by using X-ray scattering. Fig. 2(b) exhibits a typical X-ray diffraction pattern of an aligned nematic liquid crystal [32] with a pronounced azimuthal distribution of intensity at $2\theta = 20.15^{\circ}$, corresponding to a dimension of lateral packing mesogenic units of about 0.44 nm. The uniaxially ordered LCE matrix creates two areas of high intensity on the meridian, which correspond to the two peaks in the azimuthal integration of wide-angle diffraction arc, as shown in Fig. 2(c). By analyzing these data, the gotten nematic order parameter is about 0.58 (see "Support Information"). In addition, the introduction of polyurethane skeleton in nematic LCE matrix brings about a broad ring in the X-ray diffraction pattern shown in Fig. 2(b), which can be identified by comparing with the X-ray diffraction pattern of the bare polyurethane porous foam shown in Fig. S1(b).

The porous structure of the LCENB and the alignment of mesogens in the LCE matrix were generated in the drawing process of the fabrication (see Experimental Section). The polyurethane porous foam is of a 3D network construction with the open porosities being mutually connected. After the first crosslinking stage, the pores within the polyurethane porous foam were fully filled with partially crosslinked swollen gel, which formed a

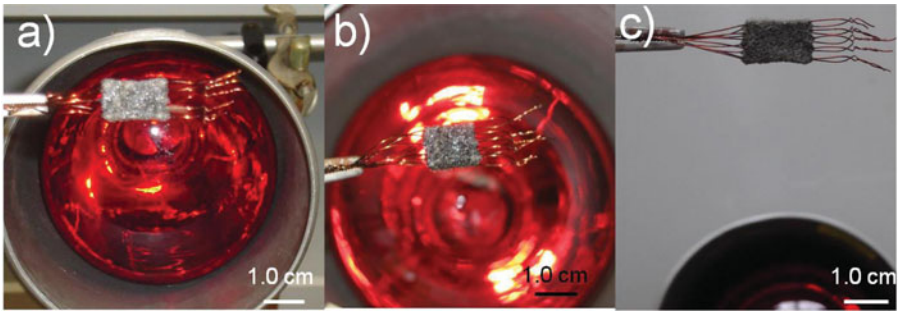

Figure 3. Optical images of the photo actuation of the LCENB. The LCENB is uniformly irradiated on four facets by rotating the bulk. The copper hooks, which were pierced at the top and the bottom edges of the bulk in the drawing process for stretching alignment, are not removed. (a) The initial state of the LCENB with the height of 1.6 cm. (b) The LCENB contracts to a stable state with a new height of 1.2 cm, 75 % of the initial value, after ∼30 s under IR irradiation with the intensity of 3.5 W/cm^2. (c) The bulk recovers to its initial dimensions ∼30 s after the IR source is removed.

continuous phase embedding the polyurethane skeleton network due to the open porosities. During the drying process, the gel shrank as the contained toluene was evaporated, and caused the polyurethane porous foam to shrink with it. During this process, the pores were also compressed. In the drawing process, the gel-filled polyurethane porous foam was stretched up to its initial height, which was framed by the PTFE mold used. The gel, being tightly adhered with the polyurethane skeleton network, was also forced to stretch with the polyurethane skeleton network. Consequently, the alignment of the mesogenic units along the stretching direction was formed. In addition, the pores in the polyurethane porous foam expanded back during the drawing process, while the gel cladding the polyurethane skeleton network became thinner during the stretching process, leading to partial release of the pores. This results in the ultimate porous structure in the nanocomposite bulk. The LCENB with 3D elastic skeleton network of polyurethane and nematic LCE/SWCNT as the matrix was finally prepared in the second crosslinking stage.

The prepared LCENB demonstrated strong reversible photo actuation. As shown in Fig. 3(a)–(c), under the irradiation of infrared (IR) light with an intensity of 3.5 W/cm^2 (the emitted light spectrum is shown in Fig. S1), the bulk contracted evenly along its height to a maximum of 25% in 30 s. During the irradiation, the LCENB was rotated to ensure a uniform irradiation of its facets. When the irradiation stopped, the bulk recovered to its initial height in about 30 s. Fully reversible contraction and restoration were thus observed under these irradiation/nonirradiation cycles. The shape deformation was induced by the change in the nematic order of the LCE matrix. Nematic LCE matrix possesses the uniaxial orientational order formed by the alignment of the mesogenic groups. When the nematic LCE is heated above or cooled down below its nematic-isotropic transition temperature (T_{ni}), the change in the degree of alignment of mesogenic rods leads to the change of the nematic order, spontaneous contraction or elongation of the whole network along the nematic director thus occurs [8]. In our LCENB, SWCNTs efficiently absorbed and converted photon energy into thermal energy [33], acting as the nanoscale heat source and thermal conduction pathway to effectively heat up the LCE matrix, elevating its temperature to above the T_{ni}, changing the nematic order, and leading to an axial contraction of LCE matrix. The measured maximum stable temperature of the LCENB under IR irradiation was about 90°C, which was above the T_{ni} of the LCE matrix [16]. This contraction of

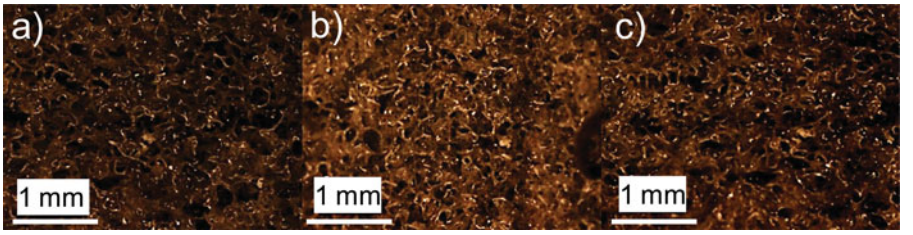

Figure 4. Optical microscopic images of the as-prepared LCENB at the normal state, the compressed state, and the stretched state respective. The orientation of compression and stretch is horizontal orientation. (a) The normal morphology of the LCENB with pores (shown as round and dark spots). (b) The morphology at the compressed state of the LCENB. Fewer and smaller spots are observed, owing to the compression of the material. (c) The morphology of the LCENB when stretched. The deformed pores become elongated along the stretched direction but narrower.

LCE compresses the elastic 3D polyurethane skeleton network, thus decreasing the height of the LCENB. After the irradiation stops and the temperature drops, a transition from the isotropic phase back to the nematic phase happens in the LCE matrix. As a result, the mesogenic groups recover to their initial alignment degree. The elastic restoration force of the 3D polyurethane skeleton network provides an axial tensile stress to the LCE matrix, which is conducive to the LCE matrix returning to its initial nematic structure and dimensions. Finally, the 3D polyurethane skeleton network and the LCE matrix fully recover to their initial states. During this reversible deformation process, the LCENB maintains its robustness performance as a solid bulk owing to the stabilizing effect of the elastic skeleton, even though the LCE matrix could be softened during its phase transition at a high temperature around T_{ni}, which was evidenced in previous work [34–36]. Therefore, the effective mechanical coupling between the elastic skeleton of the 3D polyurethane network and the nematic LCE matrix, which are well compatible with each other, is one critical factor for the reversible actuation and deformation of the LCENB. On the other hand, the axial contraction of the nematic LCE causes its expansion in other orthogonal directions [37]. The porous structure in the nematic LCENB provides free spaces to realize this shape deformation of the LCE matrix, while also reducing the spatial hindrance to the elastic deformation of the skeleton network. Hence, the porous structure plays another critical role in the LCENB for its fully reversible actuation. Figure 4 shows the deformation of the pores caused by the deformation of LCENB.

When the LCENB was asymmetrically irradiated from one side by a white light source with the intensity of 250 mW/cm^2 (the emitted light spectrum is shown in Fig. S3), as shown in Fig. 5(a)–(c), the heat transfer resistance due to the thickness of the bulk resulted in a temperature gradient between the two sides of the bulk: the side facing the irradiation was heated up above the T_{ni} while the temperature of the opposite side was lower. As a result, the LCENB could bend towards the incident light. The bending was up to 40°within 40 s, and recovered to its initial erect state in about 40 s after the light source was switched off.

Based on its photo actuation performance, we next implemented the LCENB as the actuator to drive a scanning mirror. The purpose is to demonstrate that our LCENB can carry a relatively heavy load and provide rotational actuation to it. Here, a piece of rectangular silicon bulk cut from a polished silicon wafer was attached to the top back of the LCENB as the mirror surface. The bottom of the LCENB was fixed on a glass substrate. The LCENB was initially set straight up and in its natural shape. Figure 6(a) illustrates the

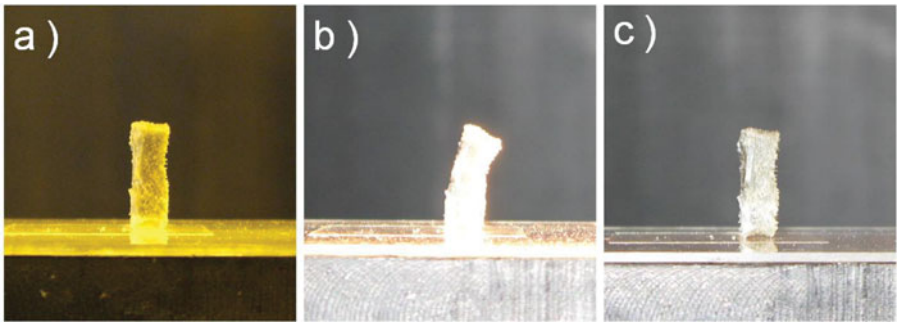

Figure 5. Optical images of the photo actuation of the LCENB. The LCENB is asymmetrically irradiated on one facet. (a) The initial erect bulk, with its bottom fixed on a glass by a double-sided adhesive tape. (b) The bulk bends toward the light source by about 40°under an irradiation of white light with the intensity of 250 mW/cm^2 within 40 s. (c) The bulk recovers to its initial erect state in about 40 s after the light source is switched off.

setup of the experiment. The mirror was illuminated by a blue laser (wavelength: 473 nm, DPSS Laser System, Laserglow Technologies, Toronto, Canada). The reflected beam was received by a screen with a printed logo. The white light source used in Fig. 5 (a)–(c) was again employed to activate the LCENB (intensity: 250 mW/cm^2). Figure 6(b) illustrates the state of the LCENB actuating the mirror when the light source was on. The LCENB bent towards the incident light, tilting the mirror, and therefore, changing the direction of the reflected beam. As a result, the mirror was able to scan through a wide angle across the screen. Figure 6(c)–(g) shows the image frame sequence of a full tuning process of the scanning mirror. At the beginning (time instant: 0 s), the LCENB is in its natural upright shape and the light source was off (Fig. 6(c)). The spot of the reflected beam on the screen was close to the bottom. After the light source was turned on, the mirror became tilted, and the reflected beam spot was higher than its initial position on the screen. This is clearly shown in Fig. 6(d) and (e), corresponding to 19 s and 26 s after the light source was turned on, respectively. As time proceeded, the beam spot further went up and beyond the range of the screen. The light source was turned off at the time instant of 35 s. The LCENB started to resume to its original shape, and thus driving the mirror to return to its initial upright state. The reflected beam then started to scan the screen in a reversed manner. A clear image of the tilted mirror is highlighted in Fig. 6(f), which was the state of the scanning mirror 10 s after the light source was turned off, and demonstrates the reverse scanning of the reflected beam. The reflected beam spot returned close to its initial position about 40 s after the light source was turned off, and arrived at its initial position 91 s after the light source was turned off, as shown in Fig. 6(g). The movie showing the operation of the scanning mirror is in the Supporting Information. In the actuation of the scanning mirror, the LCENB demonstrated excellent characteristic performance as a bulk actuator that can carry an object to move back and forth, in stark contrast to other LCE-based actuators in forms of films or fibers, which generally only provide traction. The nematic LCEs can effectively generate pulling force during their contraction process, but generally cannot provide enough reversed pushing force when stretching back. For example, in a previously reported device [38], a microgripper was constructed based on LCE materials with silicone rubber joints and a mirror attached to the arms in order to measure the position of the arms during the actuation process by using a laser. The clamping process of the microgripper

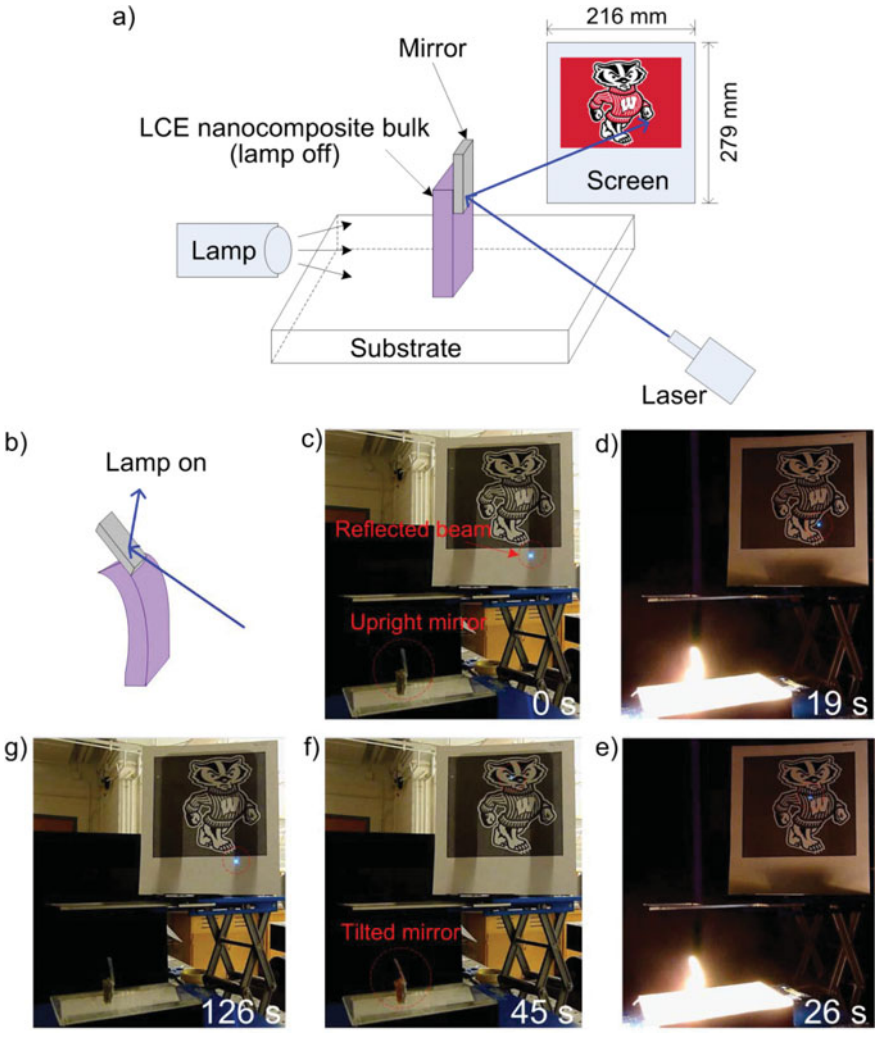

Figure 6. The operation of a scanning mirror actuated by the LCENB. (a) A schematic setup of the photo-driven scanning mirror system. (b) A schematic showing the state of the LCENB actuating and tilting the scanning mirror when it is irradiated by light. (c–g) Images of the photo-driven scanning mirror system. A spot due to the laser beam reflected from the scanning mirror moved along the screen during the scanning process. (c) The initial state before the light source was turned on; (d) 19 s after the light source was turned on; (e) 26 s after the light source was turned on; (f) At the time instant of 45 s, or 10 s after the light source was turned off; (g) the complete mirror system recovered to its initial state at the time instant of 126 s, or 91 s after the light source was turned off.

was driven by the contraction of LCE films, but its unfolding process was dependent on the elasticity of the silicon rubber. In the reversible actuation of our LCENB, the pulling force also stems from the contraction of the LCE matrix. During the recovering process, however, with the elasticity of the 3D polyurethane skeleton network, the LCENB fully restores to its original state, while providing enough reversed actuation force to the load, thus realizing a performance of carrying an object to move back and forth.

4. Conclusions

We have developed a bulk LCE material using a procedure of two-stage crosslinking coupled with a drawing process. The LCENB consists of a 3D elastic skeleton network of polyurethane and a polysiloxane-based nematic LCE incorporated with SWCNTs as the matrix. It can be reversibly actuated by light with high sensitivity. Under a uniform irradiation, the bulk could contract by 25% in its height. Under an asymmetrical irradiation, the bulk could bend by as much as 40°. Based on our LCENB, we demonstrated a mirror device with large scanning range. Our material synthesis approach can be extended to make bulk materials of other polysiloxane-based LCEs. The extent of activated shape deformation of the LCENB may be further increased by using a nematic LCE with a much higher uniaxial contraction ratio as the matrix, such as the main-chain LCEs [36, 39], or side-chain LCEs with long-chain cross linker connecting the siloxane polymer chains [40]. The response rate of the bulk material can be improved by optimizing the type and structure of the materials used in nanocomposites to increase the absorption of light.

Acknowledgments

This research utilized NSF-supported shared facilities at the University of Wisconsin. The authors thank N. L. Abbott, Z. Q. Yang and Y. Liu for academic communications.

Funding

This work was funded by the University of Wisconsin – Madison Vilas Associates Program supported by the Vilas Trustees, and partly by Wisconsin Institutes for Discovery and the U.S. National Science Foundation under Grant ECCS 0702095.

Supporting Data

Supplemental data for this article can be accessed at http://www.tandfonline.com/gmcl

References

[1] Smela, E. (2003). *Adv. Mater.*, *15*, 481.
[2] Ahir, S. V. & Terentjev, E. M. (2005). *Nature. Mater.*, *4*, 491.
[3] Dong, L., Agarwal, A. K., Beebe, D. J., & Jiang, H. R. (2006). *Nature*, *442*, 551.
[4] Alexander, C. & Shakesheff, K. M. (2006). *Adv. Mater.*, *18*, 3321.
[5] Yu, Y. & Ikeda, T. (2006). *Angew. Chem. -Int. Ed.*, *45*, 5416.
[6] Donnio, B., Wermter, H., & Finkelmann, H. (2000). *Macromolecules*, *33*, 7724.
[7] Ohm, C., Brehmer, M., & Zentel, R. (2010). *Adv. Mater.*, *22*, 3366.
[8] Warner, M. & Terentjev, E. M. (2003). *Liquid Crystal Elastomers*. Oxford University Press: Oxford.
[9] Yu, Y., Nakano, M., & Ikeda, T. (2003). *Nature*, *425*, 145.
[10] Ikeda, T., Mamiya, J. I., & Yu, Y. (2007). *Angew. Chem.-Int. Edit.*, *46*, 506.
[11] Yang, L., Setyowati, K., Li, A., Gong, S., & Chen, J. (2008). *Adv. Mater.*, *20*, 2271.
[12] Xu, S., Ren, H., Lin, Y., Moharam, M. G. J., Wu, S., *et al.* (2009). *Opt. Express*, *17*, 17590.
[13] Serak, S., Tabiryan, N., Vergara, R., White, T. J., Vaia, R. A., *et al.* (2010). *Soft Matter*, *6*, 779.
[14] Cheng, F., Yin, R., Zhang, Y., Yen, C., & Yu, Y. (2010). *Soft Matter*, *6*, 3447.
[15] Ji, Y., Huang, Y., Rungsawang, R., & Terentjev, E. M. (2010). *Adv. Mater.*, *22*, 3436.
[16] Li, C., Liu, Y., Lo, C-W., & Jiang, H. (2011). *Soft Matter*, *16*, 7511.
[17] Yu, H. & Ikeda, T. (2011). *Adv. Mater.*, *23*, 2149.

[18] Wu, W., Yao, L., Yang, T., Yin, R., Li, F., *et al.* (2011). *J. Am. Chem. Soc.*, *133*, 15810.
[19] Wang, W., Sun, X., Wu, W., Peng, H., & Yu, Y. (2012). *Angew. Chem. -Int. Ed.*, *51*, 4644.
[20] Marshall, J. E., Ji, Y., Torras, N., Zinoviev, K., & Terentjev, E. M. (2012). *Soft Matter*, *8*, 1570.
[21] Ryabchun, A., Bobrovsky, A., Stumpe, J., & Shibaev, V. (2012). *Macromol. Rapid Commun.*, *33*, 991.
[22] Li, C., Liu, Y., Huang, X., & Jiang, H. (2012). *Adv. Funct. Mater.*, *22*, 5166.
[23] Jiang, Y., Xu, D., Li, X., Lin, C., Li, W., *et al.* (2012). *J. Mater. Chem.*, *22*, 11943.
[24] Kohlmeyer, R. R. & Chen, J. (2013). *Angew. Chem.-Int. Edit.*, *52*, 9234.
[25] Naciri, J., Srinivasan, A., Jeon, H., Nikolov, N., Keller, P., *et al.* (2003). *Macromolecules*, *36*, 8499.
[26] Ahir, S. V., Tajbakhsh, A. R., & Terentjev, E. M. (2006). *Adv. Funct. Mater.*, *16*, 556.
[27] Yoshino, T., Kondo, M., Mamiya, J., Kinoshita, M., Yu, Y., *et al.* (2010). *Adv. Mater.*, *22*, 1361.
[28] Ohm, C., Morys, M., Forst, F. R., Braun, L., Eremin, A., *et al.* (2011). *Soft Matter*, *7*, 3730.
[29] Liu, D., Bastiaansen, C. W. M., den Toonder, J. M. J., & Broer, D. J. (2012). *Angew. Chem.-Int. Edit.*, *51*, 892.
[30] Ji, Y., Marshall, J. E., & Terentjev, E. M. (2012). *Polymers*, *4*, 316.
[31] Jiang, H., Li, C., & Huang, X. (2013). *Nanoscale*, *5*, 5225.
[32] Greve, A. & Finkelmann, H. (2001). *Macromol. Chem. Phys.*, *202*, 2926.
[33] Ajayan, P. M., Terrones, M., de la Guardia, A., Huc, V., Grobert, N., *et al.* (2002). *Science*, *296*, 705.
[34] Finkelmann, H., Greve, A., & Warner, M. (2001). *Eur. Phys. J. E.*, *5*, 281.
[35] Clarke, S. M., Hotta, A., Tajbakhsh, A. R., & Terentjev, E. M. (2002). *Phys. Rev. E.*, *65*, 021804.
[36] Zander, F. & Finkelmann, H. (2010). *Macromol. Chem. Phys.*, *211*, 1167.
[37] Sanchez-Ferrer, A., Fischl, T., Stubenrauch, M., Albrecht, A., Wurmus, H., *et al.* (2011). *Adv. Mater.*, *23*, 4526.
[38] Sánchez-Ferrer, A., Fischl, T., Stubenrauch, M., Wurmus, H., Hoffmann, M., *et al.* (2009). *Macromol. Chem. Phys.*, *210*, 1671.
[39] Krause, S., Zander, F., Bergmann, G., Brandt, H., Wertmer, H., *et al.* (2009). *C. R. Chim.*, *12*, 85.
[40] Tajbakhsh, A. R., & Terentjev, E. M. (2001). *Eur. Phys. J. E.*, *6*, 181.